Berson A., Brown P.S., Talbot E.L., Badyal J.P.S., Bain C.D. (2011) Experimental investigation of the impact, spreading, and drying of picolitre droplets onto substrates with a broad range of wettabilities, NIP27, 27th International Conference on Digital Printing Technologies, Minneapolis, USA, October 2-6, 2011.

Experimental investigation of the impact, spreading and drying of picolitre droplets onto substrates with a broad range of wettabilities

Arganthaël Berson, Emma L. Talbot, Philip S. Brown, Colin D. Bain; Department of Chemistry, Durham University; Durham, UK, DH1 3LE

Abstract

The effect of the substrate wettability on the deposition of picolitre droplets by drop-on-demand technology is investigated experimentally. Substrates with a broad range of wettabilities are considered with contact angles ranging from 19° *for water on glass to* 118° *for water on a super-hydrophobic plasma-treated glass slide.*

Droplet profiles are recorded using high-speed imaging. The effect of surface wettability on the drying of water droplets is investigated and compared with models and experiments from the literature. Results are presented for picolitre droplets and experimental conditions relevant to inkjet printing. The cases of the pinned contact line and the moving one with a constant contact angle are both addressed.

For colloidal fluids, the formation of the deposit is further investigated using an inverted microscope coupled to a particle-tracking velocimetry system. This experimental technique allows us to track individual solute particles during the various stages of the deposition. Preliminary results show the promise of this technique for characterizing internal flows within the droplet.

Introduction

For inkjet printing applications, control of the drying of an evaporating droplet and the morphology of the resulting deposit is crucial. It is therefore necessary to understand the basic processes underlying the drying of inkjet droplets and, for colloidal solutions, to develop experimental tools to investigate the mechanisms governing internal flows and their influence on the final deposit. The drying of sessile droplets has been the object of a number of works in the past decade, including Refs. [2, 3, 5, 7] among many others. It is commonly assumed that droplet evaporation is controlled by diffusion as in the theoretical work by Popov [7], which we will take as a reference throughout the rest of this article. Despite many studies on droplet evaporation, the validity of the model by Popov has only recently been demonstrated across a wide range of contact angles for microlitre droplets [4]. The first part of this study presents experimental results for the drying of picolitre droplets, a scale more relevant to inkjet printing. Experimental data obtained on surfaces with a wide range of wettabilities are compared with evaporation models for two modes of drying: pinned contact line [7] and moving contact line with a constant contact angle.

Depending on the application, it may be required that the final deposit should be as homogeneous as possible, e.g. for conductive tracks, or, at least, of controlled geometry. The characteristics of the final deposit are strongly related to the drying conditions and more specifically to internal flows, e.g. evaporation-driven flow, Marangoni flow. The well-known "coffee-ring" effect, for instance, results from the strong evaporative flux near the contact line that drives the fluid (and solid particles) away from the droplet centre, thus forming a ring-shaped deposit [2]. Recently, several studies have started to measure internal flows quantitatively in drying droplets but they focus on the microlitre scale, e.g. [1, 6]. The second part of this study presents preliminary results for the characterization of internal flows inside a drying picolitre droplet. The velocity fields are measured using particle-tracking velocimetry and compared with theoretical predictions.

Drying of water droplets on various solid substrates.

In this section, we investigate the drying of picolitre water droplets on a variety of solid substrates covering a range of apparent contact angles between 20° and 120°.

Evaporation model

In order to describe the evaporation of a picolitre water droplet sitting on a solid substrate, we follow the theoretical approach proposed by Popov [7]. Similar to the earlier work by Deegan et al. [2, 3], the model by Popov assumes that the evaporation of the droplet is governed by diffusion of the vapour from the droplet interface to the ambient atmosphere. In this case, it is demonstrated that the evaporative flux is not constant along the liquid-gas interface and that evaporation is stronger near the contact line.

The droplet has the shape of a spherical cap, which is a reasonable assumption given the low value of the Bond number ($\approx 10^{-4}$) for such small droplets. Therefore, the mass M of the droplet is given by

$$M = \rho_f \pi R^3 \frac{\cos^3\theta - 3\cos\theta + 2}{3\sin^3\theta}, \tag{1}$$

where ρ_f is the density of the fluid, R is the radius of the circle formed by the contact line, amd θ is the apparent contact angle.

Assuming no thermal effect, no Marangoni flow and a quasi-steady process so that at each instant the shape of the droplet and the corresponding evaporative flux are calculated based on equilibrium conditions, the evaporation rate is given by [7]

$$\frac{dM}{dt} = -\pi R D(n_s - n_\infty)\left[\frac{\sin\theta}{1+\cos\theta} + 4\int_0^\infty \frac{1+\cosh(2\theta\tau)}{\sinh(2\pi\tau)}\tanh((\pi-\theta)\tau)d\tau\right], \quad (2)$$

where D is the diffusivity of water vapour in air, n_s is the saturation vapour density of the fluid and n_∞ is the vapour density in the ambient atmosphere, far from the droplet ($n_\infty = RH \times n_s$, with RH the ambient relative humidity).

When the contact line is pinned, the radius R of the droplet is constant and the contact angle varies with time. The combination of Equations 1 and 2 gives the following differential equation governing the evolution of the contact angle during drying [7]:

$$\frac{d\theta}{dt} = -\frac{D(n_s - n_\infty)}{\rho_f R^2}(1+\cos\theta)^2\left[\frac{\sin\theta}{1+\cos\theta} + 4\int_0^\infty \frac{1+\cosh(2\theta\tau)}{\sinh(2\pi\tau)}\tanh((\pi-\theta)\tau)d\tau\right]. \quad (3)$$

Equation 3 is solved numerically using a fourth-order Runge-Kutta algorithm (using the function *ode45* in Matlab). The drying time $t_{f,R}$ is determined when the contact angle reaches zero. For hydrophilic surfaces, it is possible to use a small-angle approximation to obtain an analytical solution of Equation 3. Using this approximation, Popov [7] found the following approximate drying time:

$$\tilde{t}_{f,R} = \frac{\rho_f \pi R^2 \theta}{16 D(n_s - n_\infty)}. \quad (4)$$

Another mode of drying is when the contact line does not pin the surface. If we assume that there is no hysteresis, the contact angle remains constant and the radius of the contact line varies. With R fixed, the combination of Equations 1 and 2 yields, after integration and using the initial radius R_0 of the contact line at the start of drying,

$$R^2 = -2\frac{D(n_s - n_\infty)}{\rho_f}\frac{\sin^3\theta}{\cos^3\theta - 3\cos\theta + 2}\left[\frac{\sin\theta}{1+\cos\theta} + 4\int_0^\infty \frac{1+\cosh(2\theta\tau)}{\sinh(2\pi\tau)}\tanh((\pi-\theta)\tau)d\tau\right]t + R_0^2. \quad (5)$$

The drying time $t_{f,\theta}$ is obtained when R=0.

Experimental

Visualisation setup

Picolitre droplets of water (ultra-high purity water) are generated using a Microfab nozzle (Horizon Instruments) with a piezoelectric driver. The diameter of the nozzle orifice is 53μm. Side-view images of drying droplets are taken using a high-speed camera (Photron APX RS) coupled to a long working distance microscope objective (20×, NA 0.4, Nikon M plan) and a tube lens ($f = +200$mm). The acquisition frequency is 400Hz, the shutter speed is 4μs and the pixel size is $0.6 \times 0.6\mu$m^2. Droplets are illuminated parallel to the axis of the camera, from the back, by a high-intensity light source (Thorlabs HPLS-30-02). Images of the droplet profiles are post-processed using in-house Matlab post-processing routines in order to extract variables such as contact-line radius, contact angle, droplet volume, etc. All these routines were validated separately and rely on the assumption that the shape of a drying droplet can be described by a spherical cap.

The temperature and relative humidity of the ambient atmosphere are critical parameters for the drying process. Temperature is monitored by a type-K thermocouple located behind the nozzle in order to reduce radiative losses related to the light source. Relative humidity is measured using a thermohygrometer (Cole Parmer). For the different datasets presented in the following, temperature varies between 32.9° and 35.5°, and the relative humidity varies between 0.40 and 0.46. The thermophysical properties of water used in the calculations are calculated based on measured temperatures and humidity ratios.

Surface preparation

Three different surfaces were used to assess the drying of picolitre droplets. The first surface (surface A) is a microscope slide, made of glass, taken from the box and rinsed with ultra-high purity water. The cleaning is not very thorough and therefore the contact angle is approximately 57° and droplets tend to pin to the surface during drying. The second surface (surface B) is a similar microscope slide but cleaned more thoroughly using Decon 90 (2w/w% in water). The contact angle is lower (approximately 19°) and both drying modes are observed (constant radius and constant contact angle). The third surface (surface C) is prepared by spin coating and annealing a solution of polybutadiene in toluene onto a polished silicon wafer. The surface subsequently undergoes plasma fluorination in the presence of CF_4 gas for ten minutes at a power of 30W. The complete procedure is described in Ref. [8]. This surface is superhydrophobic and yields a contact angle of approximately 170° for large droplets (μL). However, for picolitre droplets, the contact angle is approximately 118°. Droplets do not pin during drying on surface C.

Results

Table 1 compares the calculated drying times, in the two different modes of drying (constant R and constant θ), with experimental data obtained for different surfaces. Contrary to what was observed for mm-sized droplets by Gelderblom et al. [4], the predicted drying times are not in good agreement with the experimental ones. The model largely underestimates the experimental results. Such large discrepancy is surprising and we are currently investigating its possible causes. The ambient temperature and humidity close to the droplet have a significant effect on the predicted drying rate. Their monitoring may not be adequate in the current setup and it will be improved in the future.

Nevertheless, a good agreement is found if the discrepancy between the experimental and theoretical evaporation rates is accounted for by normalizing the data. Figures 1 to 3 show the droplet mass normalized by its initial value as a function of a dimensionless time t/t_f during evaporation on different surfaces. As predicted by the model by Popov, the mass of a pinned droplet decreases almost linearly when the contact angle is small ($\theta = 19°$) but becomes nonlinear at larger contact angles ($\theta = 57°$ and 118°). In the constant-contact-angle mode, the mass of the

Predicted and experimental drying times for the three surfaces under test. V is the droplet volume. Observed drying modes are either pinned contact line ($R = ct$) or constant θ ($\theta = ct$).

	θ (°)	V (pL)	$t_{f,R}$ (s)	$\tilde{t}_{f,R}$ (s)	$t_{f,\theta}$ (s)	$t_{f,exp}$ (s)	mode
A	57	24	0.31	0.29	0.41	0.67	$R = ct$
B	19	13	0.15	0.15	0.20	0.54	both
C	118	8	0.20	0.10	0.21	0.91	$\theta = ct$

droplet decreases nonlinearly regardless of the contact angle.

For all the surfaces tested here and for both drying modes, there is a very good agreement between the model and the experimental results when the data is normalized. The difference between the two modes is most visible in Figure 2, for surface B, where two droplets with a moving contact line and one pinned droplet show very different drying behaviour. The models predict that drying should be faster for pinned droplets than in the constant-contact-angle mode. Indeed, the drying time is approximately 30% longer for surfaces A and B. However, it is almost the same for surface C so the difference between the two modes seems more important for droplets with a small contact angle.

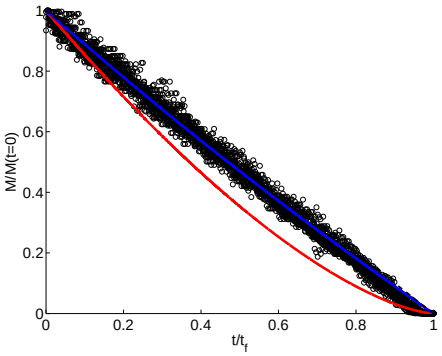

Figure 1. *Normalized mass as a function of normalized time during drying on surface A ($\theta = 57°$). The blue line is the model prediction for the pinned-contact-line mode. The red line is the model prediction for the constant-contact-angle mode. The black dashed line is a guide for the eye representing a linear decrease of the droplet mass. Experimental data are for ten droplets. All the droplets stayed pinned during most of the drying process.*

Advanced measurements techniques for the characterization of internal flows

In this section, we present preliminary results concerning the development of advanced measurement techniques for the characterization of internal flows during the drying of inkjet droplets.

Experimental

Picolitre droplets of water are generated using the same device as described in the previous section and jetted onto a regular microscope slide (glass, surface A). An inverted microscope has been developed in order to take images of the droplets through the substrate, from below. A long-working distance objective lens (50×, NA= 0.55) is coupled to a digital video camera (JVC TK-

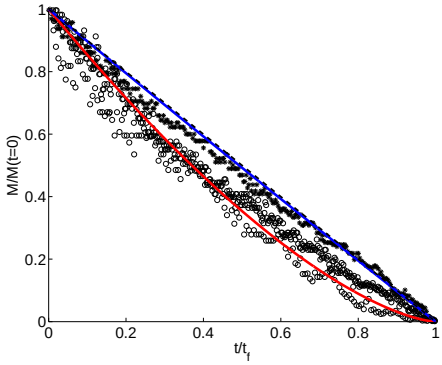

Figure 2. *Normalized mass as a function of normalized time during drying on surface B ($\theta = 19°$). Experimental data are for three droplets. One droplet stayed pinned during the drying process (stars), the others dried according to the constant-contact-angle mode (circles). Colours are the same as in Figure 1*

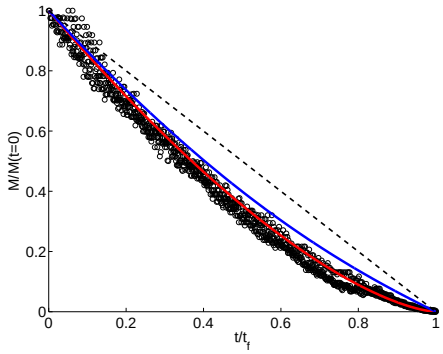

Figure 3. *Normalized mass as a function of normalized time during drying on surface C ($\theta = 118°$). Experimental data are for three droplets. All the droplets dried according to the constant-contact-angle mode. Colours are the same as in Figure 1*

S350EG) aquiring images at the rate of 25Hz. The droplet is illuminated from above by a blue LED light source. The angle of incidence of the light source is adjusted in order to minimize reflections in the field of view. Images are taken in a plane close to the substrate but not accurately determined.

The droplet is seeded with polystyrene spheres (Bangs Laboratories), with a diameter of 395nm at a concentration of 0.01w/w%. These solid particles scatter light and they are used as tracers to follow the flow inside the drying droplets. Images are exported into Matlab and the location of tracer particles is detected to a sub-pixel accuracy. The displacement of the particles between images is calculated using a particle-tracking algorithm [9], which yields velocity fields inside the drying droplet.

An example of an image obtained with this setup is provided in Figure 4. In addition to convective motion, tracer particles undergo Brownian motion. In order to separate between convective flow and Brownian motion, it is necessary to average the velocity fields either in time or in space. Indeed, since Brownian motion makes particles move in random directions, its contribution to the average velocity is nil and we are left with only the contribution of the convective flow. We take advantage of the axisymmetry of the

droplet and convert velocity fields in polar coordinates. Velocity fields are subsequently averaged spatially within the four regions depicted in Figure 4. In our experiments, no more than 25 tracer particles are identified in each region. Future experiments will include a larger number of tracers in order to improve the quality of the data.

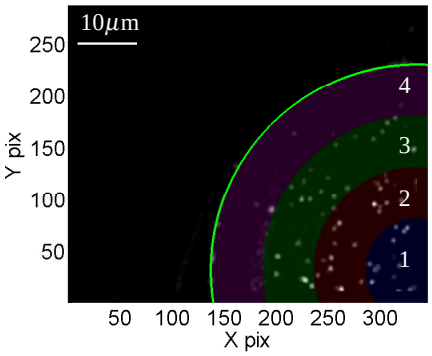

Figure 4. *Example of image obtained with the inverted microscope. The green line indicates a circular fit of the contact line. The inside of the droplet is separated into four different regions for spatial averaging.*

Results

Figure 5 shows the evolution of the radial velocity during drying averaged over the four regions defined in Figure 4. The velocity in regions 1 and 4 seems to remain close to zero throughout drying. This is expected in region 1, which is close to the centre of the droplet where velocity is expected to be small. Region 4 suffers from an insufficient number of detected tracers and it is difficult to draw conclusions. However, the velocity increases exponentially near the end of drying in regions 2 and 3. The divergence of the velocity field is due to a stronger evaporation near the contact line with respect to the apex of the droplet. This evaporation-driven flow drives particles towards the contact line and it is responsible for the well-known "coffee-ring" effect [2, 3, 5]. According to the theory [3, 5], the velocity is expected to increase as $(1-t/t_f)^a$, where $a=-1$. The exponent a is obtained from our experimental data using a linear fit (Figure 5, insert). We obtain $a \approx -1.07$, which is in good agreement with the theory.

Conclusion

In a first part, the drying of picolitre water droplets on a range of surfaces has been investigated. We compared our experimental results with diffusion-controlled evaporation models for two modes of drying: pinned contact line and constant contact angle. Droplet mass decreases linearly when the contact line is pinned and the initial contact angle is small. However, the decrease becomes more nonlinear for pinned droplets with larger contact angles and in the constant-contact-angle mode, regardless of the contact angle. Droplets are expected to dry faster when they are pinned throughout drying, especially for low contact angles. The models overpredict the evaporation rate and experiments are in progress to determine the cause of this discrepancy.

The second part of the paper presented preliminary results regarding the characterization of internal flows in a drying droplet using particle-tracking velocimetry. As expected, the flow is directed radially towards the contact line and the velocity diverges at the end of drying. The exponent of the velocity increase was measured and it is in good agreement with theory. The experimental setup is currently being improved in order to increase the image quality and the time resolution of the measurements.

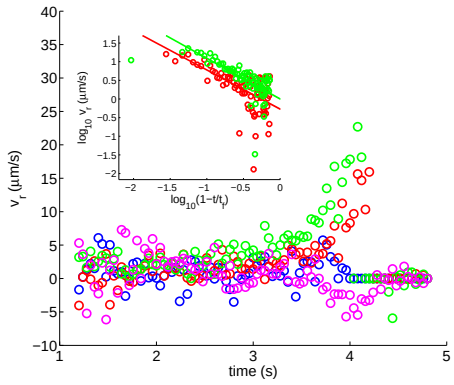

Figure 5. *Evolution of the radial velocity inside the droplet with time during drying. The velocity is space-averaged inside regions 1 (blue), 2 (red), 3 (green) and 4 (magenta). Insert: Radial velocity inside regions 2 and 3 in logarithmic scale for comparison with the theory. Linear fittings yield* $a = -1.05$ *in region 2 and* $a = -1.09$ *in region 3.*

Acknowledgments

This work received financial support from EPSRC under grant number EP/H018913/1. The help and support provided by Prof. Jas Pal Badyal are also gratefully acknowledged.

References

[1] Bodiguel H., Leng J., Soft Matter, 6, pp. 5451–5460 (2010).

[2] Deegan R.D., Bakajin O., Dupont T.F., Huber G., Nagel S.R., Witten T.A., Nature, 389, pp. 827–829 (1997).

[3] Deegan R.D., Bakajin O., Dupont T.F., Huber G., Nagel S.R., Witten T.A., Phys. Rev. E, 62(1), pp. 756–765 (2000).

[4] Gelderblom H., Marín Á.G., Nair H., van Houselt A., Lefferts L., Snoeijer J.H., Lohse D., Phys. Rev. E, 83, 026306 (2011).

[5] Hu H., Larson R.G., Langmuir, 21, pp.3963–3971 (2005).

[6] Kajiya T., Kaneko D., Doi M., Langmuir, 24(21), pp. 12369–12374 (2008).

[7] Popov Y.O., Phys. Rev. E, 71, 036313 (2005).

[8] Woodward I., Schofield W.C.E., Roucoules V., Badyal J.P.S., Langmuir, 19(8), pp. 3432–3438 (2003).

[9] http://physics.georgetown.edu/matlab/

Author Biography

Arganthaël Berson received his PhD in acoustics from LMFA, École Centrale de Lyon, France. He then worked at the Fuel Cell Research Centre at Queen's University in Kingston, ON, Canada, before joining Durham University, UK, in 2010 as a post-doctoral fellow. His interests include sustainable energy systems (thermoacoustic devices, fuel cells), the development of advanced flow diagnostic techniques, multiphase flow and inkjet printing.